the remaining, unacquired dataset. We can also define the resolution matrices $R^C = (G^C)^{-g} G^C$ and $R^0 = (G^0)^{-g} G^0$. The i-th electrode configuration in the unacquired dataset is considered to provide important information if it generates a large value of the *goodness function* $\Psi(i)$, where

$$\Psi(i) = \sum_{j=1}^{pq} \frac{|G_{ij}^1|}{G_j} \left[1 - \frac{R_{jj}^0}{R_{jj}^C} \right]. \tag{4.47}$$

The normalization factor

$$G_j = \frac{1}{D} \sum_{i=1}^{d} |G_{ij}^C| \tag{4.48}$$

compensates for the natural tendency of near-surface cells to dominate the sensitivity calculation. Note that $\Psi(i)$ is large when the elements of the corresponding row of matrix G^1 are large. Since a diagonal element $R_{jj} = 1$ indicates a perfect resolution of the j-th model parameter, the term $1 - R_{jj}^0 / R_{jj}^C$ appearing in Equation (4.47) forces the goodness function $\Psi(i)$ to favor electrode configurations that can constrain unresolved model parameters.

The goodness function $\Psi(i)$ in Equation (4.47) is only one of many that could be usefully defined in an optimal experimental design. We can rank the electrode configurations in the unacquired dataset according to their values of the goodness function. The ones that generate the highest goodness function are then used to generate the next dataset. An electrode configuration is rejected if it is linearly independent (as determined by their respective rows in the comprehensive Jacobian matrix) to a configuration used in the initial dataset. An example of optimized inversion using the synthetic example is shown in Figure 4.23, right panel.

4.11 Underwater resistivity techniques

A review of developments in marine electrical and electromagnetic geophysical techniques, including resistivity, IP, and EM methods, is provided by Butler (2009). A summary of the literature shows that there has developed in recent years two common modes of operation for underwater resistivity surveys. In a mode of operation (Day–Lewis *et al.*, 2006; Passaro, 2010) that is particularly suited for a number of shallow-water applications including mapping coastal freshwater discharge and nautical archaeology, an array of floating electrodes is towed on the water surface behind a vessel (Figure 4.24). Such systems can achieve continuous resistivity profiling of the subbottom resistivity structure and have detected seabed anomalies caused by shipwrecks. Other studies have attempted to use bottom-towed electrode arrays but these can be easily damaged as they are dragged across the rugged seafloor.

In another mode of operation, the electrode array is stationary. In some cases an array of grounded electrodes is employed that makes direct electrical contact with the subbottom, as in conventional land surveys. In deeper water, electrodes may be suspended on vertical cables extending from buoys or a vessel at the sea surface into the water column. This approach was used by Baumgartner and Christensen (1998). The choice of which marine

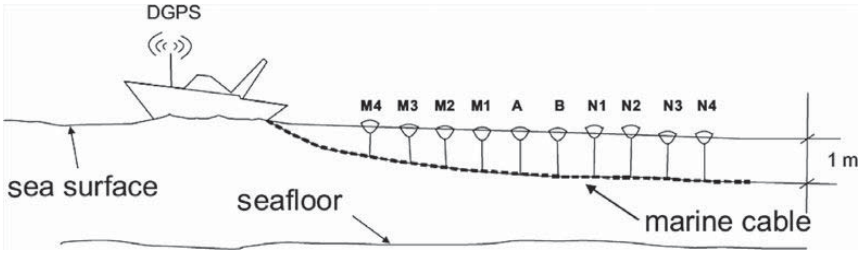

Figure 4.24 A surface-towed electrode array for marine resistivity surveys. DGPS = differential GPS navigation system. After Passaro (2010).

resistivity survey geometry to adopt for a particular project should be dictated by forward modeling of the sensitivity of the apparent resistivity pseudosection to perturbations in the expected geological scenarios, as well as logistical and budget constraints.

4.12 Illustrative case histories

Example. Tunnel construction in the Alps.

Geophysical investigations using the resistivity method were carried out in the Col di Tenda region of the Alps near the Italy–France border where the construction of a new highway tunnel is planned. Better information on the subsurface geology is required in order to determine accurate geotechnical rock-mass quality parameters so that the safety of the excavation and long-term integrity of the finished structure is ensured. A resistivity section oriented perpendicular to the planned tunnel route is shown in Figure 4.25a. Electrode spacing is 12.0 m and depth of penetration is ~ 200–300 m.

The interpretation of the resistivity section (Figure 4.25b) is based on geological outcrop and stratigraphy from boreholes. High-angle normal faults, pervasive in this region, cause the sharp lateral resistivity contrasts seen in the geoelectric section. The low-resistivity zone at the base of the fault-bounded central graben is caused by fluid circulation within an intensely fractured Jurassic limestone layer which underlies higher-resistivity Eocene calcarenites. These resistivity and complementary seismic data were able to provide detailed structual and geological information to assist the planning of this major civil-engineering project.

Example. Brownfield redevelopment.

Many urban areas contain abandoned sites that are legacies from past industrial activities. These sites often contain hazardous materials, such as polycyclic aromatic hydrocarbons and heavy metals, in addition to rubble, metal scraps, old building foundations, and other construction debris. Often it is desired to rehabilitate these sites for re-use such as commercial or residential redevelopment. Boudreault *et al*. (2010) have described geophysical work performed at such a site in downtown Montreal, Canada (Figure 4.26a)

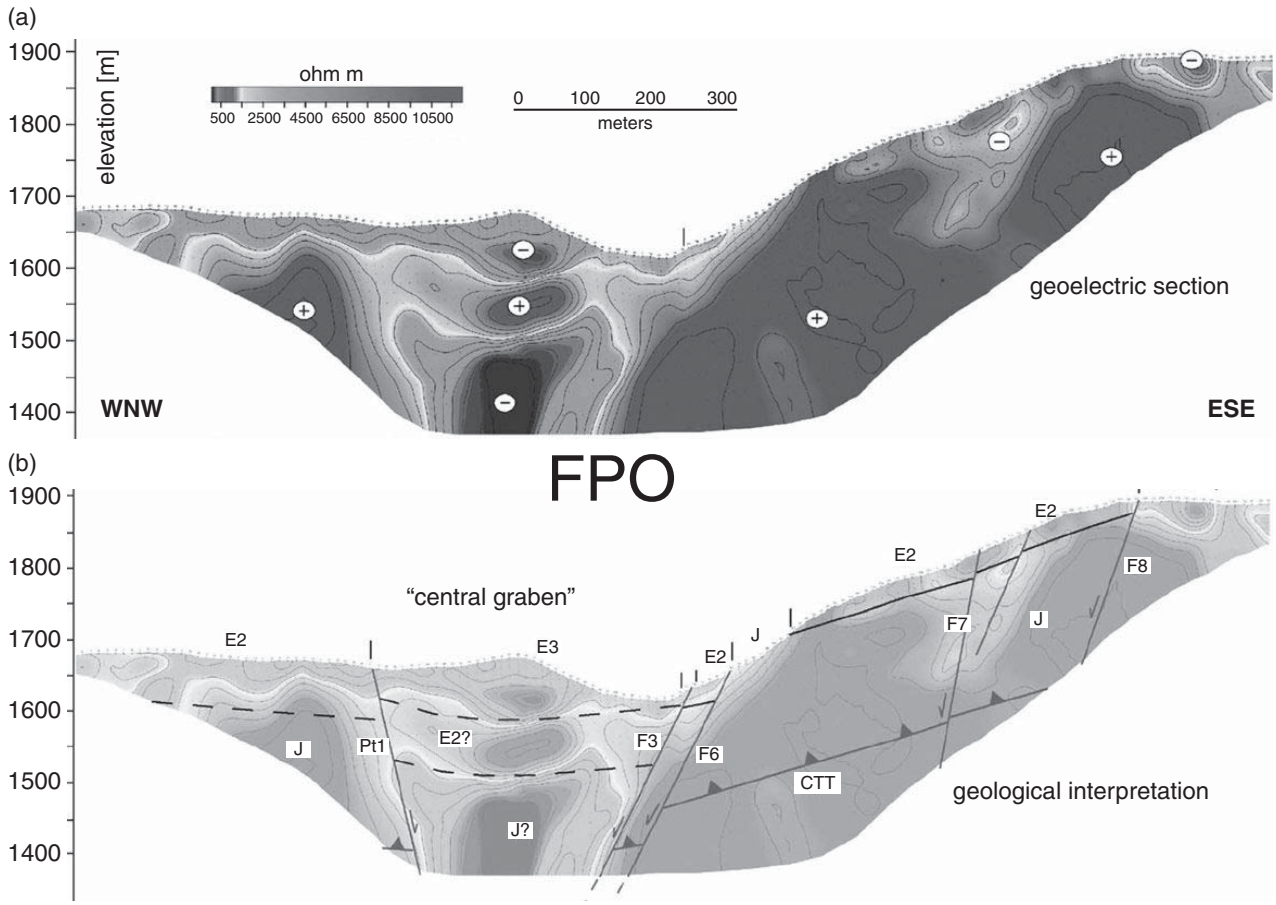

Figure 4.25 (a) Resistivity section for design of tunnel construction in Italian Alps. (b) Geological interpretation. J = Jurassic formation; E,F = Eocene formations. After Cavinato *et al*. (2006).

where new commercial development is reclaiming a long-disused parcel of urban real estate. The site is characterized by abundant heterogeneous urban fill (Figure 4.26b) that trench excavations have shown to occupy the upper ~ 2 m beneath the surface. A total of six ERT profiles were acquired, two of which are indicated in Figures 4.26c, d. The ERT images show that the upper fill layer is of higher resistivity than the underlying low-resistivity layer of natural soil. The upper layer is also strongly heterogeneous reflecting the unorganized spatial distribution of the constituent concrete and brick debris. The upper layer is more resistive than the underlying natural soil since construction materials such as brick and soil are inherently resistive (up to 1000 Ωm) compared to the natural soil and, furthermore, the upper layer is less compacted than the underlying soil and therefore has a much smaller water retention capacity, raising its resistivity. This case study shows that electrical geophysics can play a significant role in the detailed subsurface characterization of brownfield sites. The information obtained using geophysics can be used for a number of purposes, for example, it enables better assessments of potential pollutant distributions and it can help to guide the safe excavation of the site as it undergoes redevelopment.

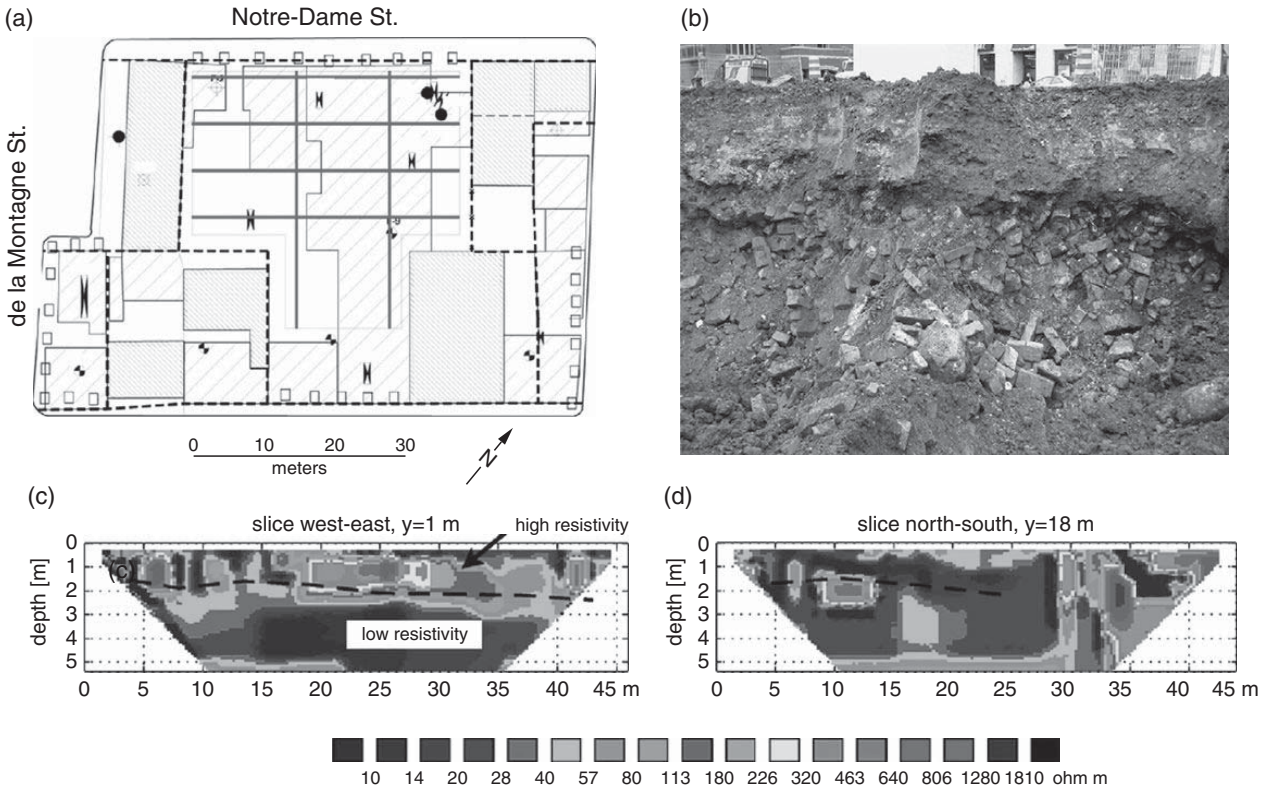

Figure 4.26 (a) Map view of urban redevelopment site, downtown Montreal, Canada. The red lines show ERT profiles. (b) Heterogeneous urban fill containing bricks, concrete, and metal debris. (c) an east–west ERT profile. (d) a north–south ERT profile. The dashed line shows the boundary between the heterogeneous fill and the natural soil, as determined by trench excavations. After Boudreault *et al*. (2010).

Problems

1. Show that the geometric factor κ for the arbitrary four-electrode arrangement is given by $\kappa = 2\pi\,[1/r_{AP}–1/r_{AQ}–1/r_{BP} + 1/r_{BQ}]^{-1}$.
2. Derive the geometric factors κ for the traditional four-electrode Schlumberger, Wenner, and dipole–dipole configurations.
3. Derive the geometric factor κ for a square array, in which the two current electrodes AB and the two potential electrodes PQ form a square of side a. Consider both cases: (i) the current electrodes are adjacent to each other; and (ii) they are diagonally opposite to each other (the *cross-square array*). Is the result of case (ii) surprising?
4. Consider a pole–pole resistivity experiment over a set of vertical fractures which can be considered as a uniform anisotropic halfspace. The potential at distance r from a point source of current I is given by

$$V(r) = \frac{I\rho_m}{2\pi r}[1 + (\lambda^2 - 1)\sin^2\varphi]^{-1/2}$$

where the coefficient of anisotropy is $\lambda = \sqrt{\rho_\perp / \rho_{||}}$ and the rms resistivity is $\rho_m = \sqrt{\rho_\perp \rho_{||}}$. The angle that the line between the current and potential electrodes makes with respect to the strike (x-direction) of the fractures is φ. Show that $V(r)$ satisfies the scaled Laplace equation

$$\frac{1}{\rho_{||}}\frac{\partial^2 V}{\partial x^2} + \frac{1}{\rho_\perp}\frac{\partial^2 V}{\partial y^2} + \frac{1}{\rho_{||}}\frac{\partial^2 V}{\partial z^2} = 0.$$

5. The apparent resistivity for the pole–pole experiment over a vertically fractured medium is measured in the along-strike and across-strike directions. (i) Prove that, in each case, the measured apparent resistivity is equal to the geometric mean of the actual resistivities in the other two directions. (ii) On a polar plot, graph the measured apparent resistivity as a function of the angle φ with respect to strike, for the case of soil-filled fractures in a weathered sandstone ($\rho_{||}$ =0.1 Ωm and $\rho_\perp$ =10 Ωm). Comment on the orientation of the resulting ellipse in terms of the *paradox of anisotropy.*
6. Consider a current electrode A placed at one corner of a square of side a. Potential electrodes P, Q, and R are placed at the other three corners, with R diagonally opposite from A. The medium is vertically anisotropic with resistivities $\rho_{||}$ and $\rho\perp$. The strike of the fractures is aligned with a side of the square. Show that the measured voltages satisfy

$$V_P^2 + V_Q^2 = \left[\frac{\rho_\perp + \rho_{||}}{\rho_m}\right]^2 V_R^2.$$